NeuroImage 82 (2013) 61–67

Contents lists available at ScienceDirect

NeuroImage

journal homepage: www.elsevier.com/locate/ynimg

Dissociation of reach-related and visual signals in the human superior colliculus

Marc Himmelbach [a,*,1], Walter Linzenbold [a,1], Uwe J. Ilg [b]

[a] Centre for Neurology, Division of Neuropsychology, Hertie-Institute for Clinical Brain Research, Centre for Integrative Neuroscience, Eberhard Karls University, Tübingen, Germany
[b] Hertie-Institute for Clinical Brain Research, Department of Cognitive Neurology, Eberhard Karls University, Tübingen, Germany

ARTICLE INFO

Article history:
Accepted 23 May 2013
Available online 30 May 2013

Keywords:
Superior colliculus
Reaching
Humans
fMRI
Vision

ABSTRACT

Electrophysiological and micro-stimulation studies in non-human animal species indicated that the superior colliculus (SC) plays a role in the control of upper limb movements. In our previous work we found reach-related signals in the deep superior colliculus in humans. Here we show that also signals in more dorsal locations are correlated with the execution of arm movements. We instructed healthy participants to reach for visual targets either presented in the left or in the right visual hemifield during an fMRI measurement. Visual stimulation was dissociated from movement execution using a pro- and anti-reaching task. Thereby, we successfully differentiated between signals at these locations induced by the visual input of target presentations on the one hand and by the execution of arm movements on the other hand. Extending our previous report, the results of this study are in good agreement with the observed anatomical distribution of reach-related neurons in macaques. Obviously, reach-related signals can be found across a considerable depth range also in humans.

Introduction

Although the cortical networks subserving upper limb functions in humans are quite well understood, the contributions of deep brain structures to the control of our arms and hands remained elusive. Our knowledge about the role of brainstem structures in the sensorimotor systems is almost entirely based on animal models. The superior colliculus, located at the dorsal brainstem, is a structure with well-known functions in the context of oculomotor control and visual processing. It contains topographical maps of the visual, auditory and somatosensory world (Cynader and Berman, 1972; Jay and Sparks, 1987; Stein et al., 2002). Additionally, the results of a small number of neurophysiological reports suggested that neurons in the SC and the directly underlying mesencephalic reticular formation are active prior to and during a reaching movement executed with the contralateral arm (Lünenburger et al., 2001; Werner et al., 1997a, 1997b). Just recently, we reported reach-related signals in the human SC, exactly replicating previous findings in animals (Linzenbold and Himmelbach, 2012).

In our previous study (Linzenbold and Himmelbach, 2012) we identified reach-related signals in deep locations of the SC contralateral to the moving arm. We also observed similar signal increases in more dorsal, presumably superficial and intermediate locations of the respective contralateral SC. However, reach-related signals in these dorsal SC locations disappeared in a comparison of reaching with the control task, i.e. execution of reflexive saccades. This finding left us with two possible interpretations. Either, these dorsal reach-related signals were exclusively driven by the visual presentation of targets in both conditions (reaching and saccades) or these signals were, at least partially, driven by the execution of arm movements and the visual stimulation and saccade execution in the control task concealed this signal source. The latter possibility is supported by the anatomical distribution of reach-related neurons throughout the depth range of the primate SC (Werner et al., 1997a, 1997b). Therefore, we dissociated arm movement signals from visual signals in the present study. We separated the visual hemifields of target presentation in individual blocks (left targets vs. right targets) and instructed the participants to execute either direct movements to the presented targets (pro-reaching) or reach to a position opposite to the presented target (anti-reaching).

In agreement with our previous results, we found reliable BOLD signal increases during right arm reaching in dorsal and ventral locations of the left human SC in all conditions (Linzenbold and Himmelbach, 2012). Thus, signals in the left dorsal SC were also clearly above baseline if there was no contralateral visual stimulation. In contrast, in the right SC we found positive BOLD signals in the dorsal location only if there was contralateral visual stimulation.

Materials and methods

Participants

Sixteen subjects (13 females, 3 males, mean age 28 years, range 23–35 years) participated in this experiment. All of them had normal

* Corresponding author. Fax: +49 7071 29 4489.
E-mail address: marc.himmelbach@uni-tuebingen.de (M. Himmelbach).
[1] Both authors contributed equally.

1053-8119/$ – see front matter © 2013 Elsevier Inc. All rights reserved.
http://dx.doi.org/10.1016/j.neuroimage.2013.05.101

or corrected-to-normal visual acuity. All participants gave their informed consent to participate in the study that was performed in accordance with the ethical standards established by the 1964 Declaration of Helsinki and approved by the local ethical committee.

Procedures

All measurements were conducted in complete darkness. We used a black, opaque film to cover all windows and panels until no light sources could be detected even after an adaptation time of ~30 min. The participants lay supine in the scanner with their heads tilted approx. 30°. They looked directly at a vertical perspex plate positioned at the level of the abdomen and used their right arm for reaching. The position of the plate was adjusted individually to ensure a comfortable movement to the targets with the index finger of the right arm. To minimise body and head movements, the right upper arm was restrained to the scanner bed. All visual stimuli were generated by LEDs located outside the scanner room and connected to optical fibres that were running to the perspex plate. Targets were positioned at 7.5°, 5°, and 2.5° to the right and to the left of the fixation position that was located at body midline. During the whole session a dimmed white central fixation light was presented. Multiple target positions were chosen to avoid the execution of automatic movements by the participants to an overlearned target location. We chose positions relatively close to the fixation because of general spatial limitations in the MR scanner and the need for a comfortable movement execution to targets in the right and left hemifield. Because of the use of a block design (see below) it was not possible to analyse the effect of target position. The fixation light was set to a level that was just sufficient to detect its position but insufficient to illuminate the workspace. The participants were instructed to maintain fixation throughout each experimental fMRI run. Reaching blocks of 17.2 s duration alternated with fixation baseline periods of the same duration. Immediately after each fixation baseline, a dimmed light next to the fixation position appeared for 2.5 s cueing the upcoming task (red for anti-reaching blocks; green for pro-reaching blocks). In the case of pro-reaching, the participants reached to the position of the flashed target, shortly touched the target with their index finger, moved back and placed their finger on a fixed home position at the sternum. In the case of anti-reaching movements, the participants executed a reaching movement to a virtual position that was exactly opposite to the actually presented targets with respect to the fixation position. These variations resulted in a 2 (target hemifield) × 2 (spatial congruency) within-subject design with the following conditions: target in the left visual field and movement to the target (LVF-PRO), target in the right visual field and movement to the target (RVF-PRO), target in the left visual field and movement opposite to the target (LVF-ANTI), and target in the right visual field and movement opposite to the target (RVF-ANTI). After each experimental block the fixation light was turned off for 500 ms indicating the end of the block. Each block consisted of 6 trials. The sequence of all reaching blocks was pseudo-randomised resulting in ITIs of max. 149 s. Each condition was repeated 4 times in one experimental run. Each participant underwent six experimental runs resulting in 144 movements per condition.

Eye and arm movement recordings

Eye movements were recorded throughout the whole fMRI measurements in both experiments with a long-range video system (SMI SensoMotoric Instruments). Video recordings of the right or left eye position, depending on eye dominance as measured by the Porta test, were sampled at 25 Hz. The synchronisation of the eye movement videos with fMRI data acquisition was ensured by the use of a TTL pulse for the start of video recording. The occurrence of occasional saccades was determined manually in a frame-by-frame analysis of the video recordings. Due to the tilted head position and the shallow viewing angle the control of eye position by eye tracking algorithms is less reliable than thorough manual inspections. The eye movement videos were analysed by an assistant who was blind to the individual sequence of experimental conditions. Two MR compatible infrared cameras positioned outside the scanner recorded the arm movements. The videos of the arm movements were sampled at 30 Hz. Onsets and offsets of the arm movements were detected and verified manually. The synchronisation of fMRI data acquisition with the hand movement videos was ensured offline by the detection of target presentations in the videos. These target presentations were controlled by a custom MatLab programme which in turn was continuously synchronised with repeated TTL pulses from the scanner.

MRI data acquisition

All experiments were conducted using a 3 T MRI scanner (Siemens Magnetom Trio, Erlangen, Germany) with a standard 12-channel head coil system. Each run consisted of 219 T2*-weighted EPI volumes (slice thickness = 2 mm, ascending acquisition of 20 slices, TR = 2.87 s including a gap of 1.5 s, TE = 33 ms, flip angle = 80°, FOV = 192 mm × 192 mm, 96 × 96 matrix) acquired in oblique coronal orientation for BOLD based imaging. Target presentations were synchronised with image acquisition and started 200 ms before the gap. The participants were instructed to execute the whole arm movement during the gap. We oriented the slices individually in parallel to the brainstem at the height of the pons. Additionally, we acquired a single whole brain EPI image from each subject with the same parameters. These images were used to facilitate the co-registration of EPI and structural datasets. Additionally, high-resolution T1-weighted anatomical volumes were acquired for each subject using an MP-RAGE sequence (TR = 1.3 s, TE = 3.22 ms, flip angle: 15, FOV = 256 mm × 256 mm, 256 × 256 matrix, 176 sagittal slices, slice thickness 1 mm).

fMRI data analysis

Image analysis was carried out using SPM8 (Wellcome Department of Imaging Neuroscience, London, UK) implemented in MATLAB 7.5 (MathWorks Inc.). The first five images of each measurement were discarded to allow the MRI signal to reach a steady state. The remaining images of each participant were realigned to the first image to correct for head movements during the experiment. The individual whole brain EPI volume was co-registered to the mean of the series of partial functional EPI images of a subject. The anatomical T1 volume was then co-registered to the whole brain EPI image. For both co-registrations we used rigid-body transformations (3 rotations, 3 translations) that were estimated based on the normalised mutual information between the respective two images, average distances between sampled points of 4 and 2 mm for repeated co-registrations with increasing precision, corresponding tolerance values of 0.02, 0.02, 0.02, 0.001, 0.001, 0.001, 0.01, 0.01, 0.01, 0.001, 0.001, and 0.001 for translations and rotations, and Gaussian smoothing of the joint histogram with 7 × 7 bins. This procedure resulted in an accurate co-registration between the functional and structural scans of our subject group (Fig. 1). Subsequently, the T1 scan was normalised to match the T1 MNI template distributed with SPM8 using the unified segmentation–normalisation approach. The calculated transformations were applied to all functional images for spatial normalisation, resampling images at a resolution of 2 × 2 × 2 mm^3. Images were smoothed with an isotropic 3 mm full-width half maximum Gaussian kernel. The fixed-effects first-level analysis included the removal of low-frequency drifts in the signal using a high pass filter with a cut-off period of 300 s and a correction for temporal autocorrelation in the data was applied using an autoregressive AR(1) process as implemented in SPM8. Predictors for each experimental condition were constructed by a convolution of arm movement onsets with the canonical haemodynamic response function. We modified the canonical haemodynamic response

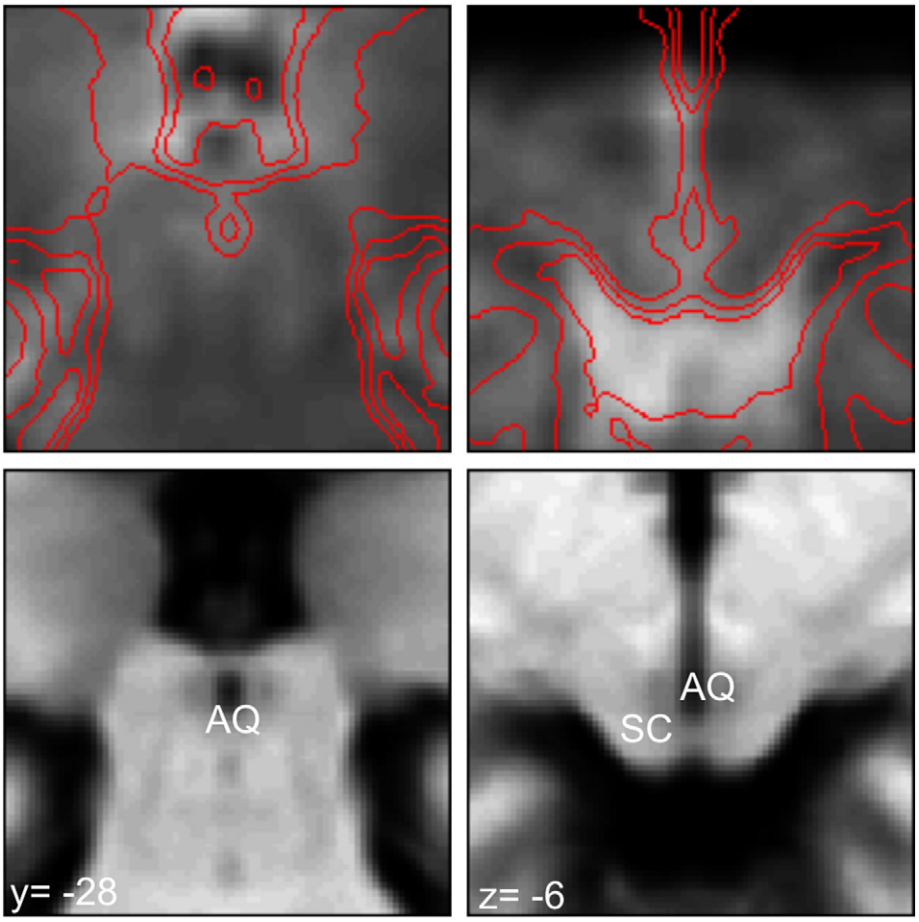

Fig. 1. Co-registration of the functional and structural group means. Contour lines were derived from the mean structural T1-weighted scan and overlaid on the mean functional EPI scan using SPM8. The MNI z-coordinate indicates the height of the transversal slices, the y-coordinate the position of the coronal slice. SC: superior colliculus, AQ: mesencephalic aqueduct.

function by changing the time-to-peak from 6 to 4 s because Wall et al. (2009) reported an equivalently shorter latency for hrf peaks at the SC upon visual stimulation. The resulting design matrices comprised 6 experimental regressors, one for each cue (pro and anti-reaching cue) and one for each of the 4 conditions of interest (i.e. LVF-PRO; LVF-ANTI; RVF-PRO; RVF-ANTI). Additionally, we included six covariates to capture residual movement-related artefacts derived from motion correction and a time series of the mean white matter signals to reduce global noise. We thresholded individual white matter masks produced by the segmentation of the T1 scan with a probability value of 0.9. Using the toolbox MarsBar (Brett et al., 2002) we read out the mean signal time course within this white matter volume mask from realigned and normalised, but unsmoothed functional images. After estimation of the model, specific effects of the experimental conditions within each participant were tested by applying linear contrasts to the parameter estimates of the events of interest.

BOLD time course extraction

In the current study we were not interested in a topographical mapping of reach-related signals, but in signal differences correlated with our experimental conditions at the locations that we previously mapped in the two experiments reported in Linzenbold and Himmelbach (2012). Therefore, we employed a region-of-interest analysis to allow for a higher signal detection power. This advantage of the region of interest analysis is based on the avoidance of the multiple comparison problem through a deliberate a priori restriction of the locations to be included in the analysis. Moreover, the equivalence of signals across conditions represented a very informative finding for our study. However, such equivalence cannot be demonstrated with a GLM approach but confidence intervals together with mean signal time courses from regions of interest can substantiate such so-called null-findings.

For each subject we defined an omnibus F-contrast comprising all four reaching conditions. Thereupon, we selected three peak signal locations from this contrast that were not more than a single voxel (2 mm) away from the group peak signal locations reported in our previous work. Please note that this process did not imply any predictions on the specific differences between conditions that were analysed later or the direction of signal changes that could be either positive or negative with respect to the fixation baseline. In this way we defined ROIs for the left deep superior colliculus (dSC) and the left and right superficial/intermediate superior colliculus (siSC). In the current experiment all participants only used the right arm. Therefore, in good agreement with our previous observations, we could not identify peak signals in the region of the right dSC. Instead, we mirrored the individual locations of the left dSC for each participant. Individual time-courses of signal intensities were extracted from a sphere with a radius of 2 mm centred at the respective voxel of each region using the toolbox NERT4SPM (Lindner and Budziszewski; http://www.hih-tuebingen.de/en/sensorimotor-lab/nod-lab/) from each subject. The individual time courses of all blocks of a given condition were aligned to the block onset and averaged within subjects. Signal intensities within each sphere were then standardised to percent signal change scale based on a 3 s pre-block baseline (averaged across all baseline blocks). Individual time courses for each condition were finally averaged across the whole group.

Results

Behavioural results

To ensure the reliability of the manual data analysis a randomly chosen subset of 27 hand movement videos was analysed by two research assistants independently from each other. We looked at the absolute time difference between movement onsets reported from both raters and found rare maximum deviations of 3 video frames. For most trials there was no difference between the raters at all or a difference of not more than a single frame. Thus, across 27 videos the mean absolute differences between raters were: LVF-PRO: 38 ms, LVF-ANTI: 39 ms, RVF-PRO: 39 ms, and RVF-ANTI: 43 ms. Differences between raters in the duration of the whole movement were even smaller on average: LVF-PRO: 25 ms, LVF-ANTI: 39 ms, RVF-PRO: 26 ms, and RVF-ANTI: 33 ms.

The analysis of the whole dataset showed that the reaction times of the participants were slightly shorter for pro- than for anti-reaching movements (LVF-PRO: Mean 303 ms (SD 73 ms); RVF-PRO: 297 (72); LVF-ANTI: 330 (85); RVF-ANTI: 338 (89)). This observation is consistent with results from previous experiments (Carey et al., 1996; Heath et al., 2009). The mean durations for complete movements including the way to the target and back to the start position across all participants and all movements were also slightly different: LVF-PRO: Mean 1148 ms (SD 155 ms); RVF-PRO: 1138 (143); LVF-ANTI: 1169 (151); RVF-ANTI: 1158 (142). All movements were indeed executed during the silent gap of EPI image acquisitions, the maximum movement duration across all participants and trials was 1470 ms. The manual inspection of the eye position video recordings did not reveal any saccades towards the target locations during the EPI data acquisition.

FMRI results

To allow for a general comparison to our previously reported data, Fig. 2 shows the result of a group GLM analysis for the deep SC location. An overview of the individual ROI coordinates together with the group coordinates reported in Linzenbold and Himmelbach (2012) is given in Table 1. The extracted time courses of the respective left and right siSC, and dSC peak locations are shown in Fig. 3 together with the respective 95% confidence intervals (CI). Signals in the right dorsal SC (siSCR) increased above baseline levels only in those two conditions that included a visual presentation of targets in the contralateral visual hemifield (Fig. 3B). We calculated the mean signal level in the siSCR for the period between 4 s and 20 s after the first movement onset in a given block. A 2 (hemifield: left vs. right) × 2 (congruency: pro vs. anti) repeated measures ANOVA of these mean values showed a significant main effect of the factor hemifield ($F_{1,15} = 42.2$, $p = 0.00001$) but no meaningful effect for the factor congruency ($F_{1,15} = 1.79$, $p = 0.20$) or the interaction of hemifield and movement ($F_{1,15} = 1.21$, $p = 0.29$). In clear contrast, in the left siSC BOLD signals increased not only for conditions with contralateral visual stimulation but also for conditions with ipsilateral visual stimulation. The confidence intervals for all conditions were clearly above baseline for the whole duration of the experimental blocks (Fig. 3A). As expected, the 2 × 2 ANOVA revealed no significant result for the main effects (hemifield: $F_{1,15} = 0.16$, $p = 0.69$; congruency: $F_{1,15} = 0.69$, $p = 0.42$) or the interaction of hemifield and movement ($F_{1,15} = 3.03$, $p = 0.10$).We found the same pattern in the left dSC ROI (Fig. 3C). The BOLD signal increased in all conditions irrespective of the hemifield of visual stimulation. A 2 × 2 ANOVA revealed no significant differences between the conditions (hemifield: $F_{1,15} = 1.04$, $p = 0.32$; congruency: $F_{1,15} = 0.12$, $p = 0.73$; interaction: $F_{1,15} =$

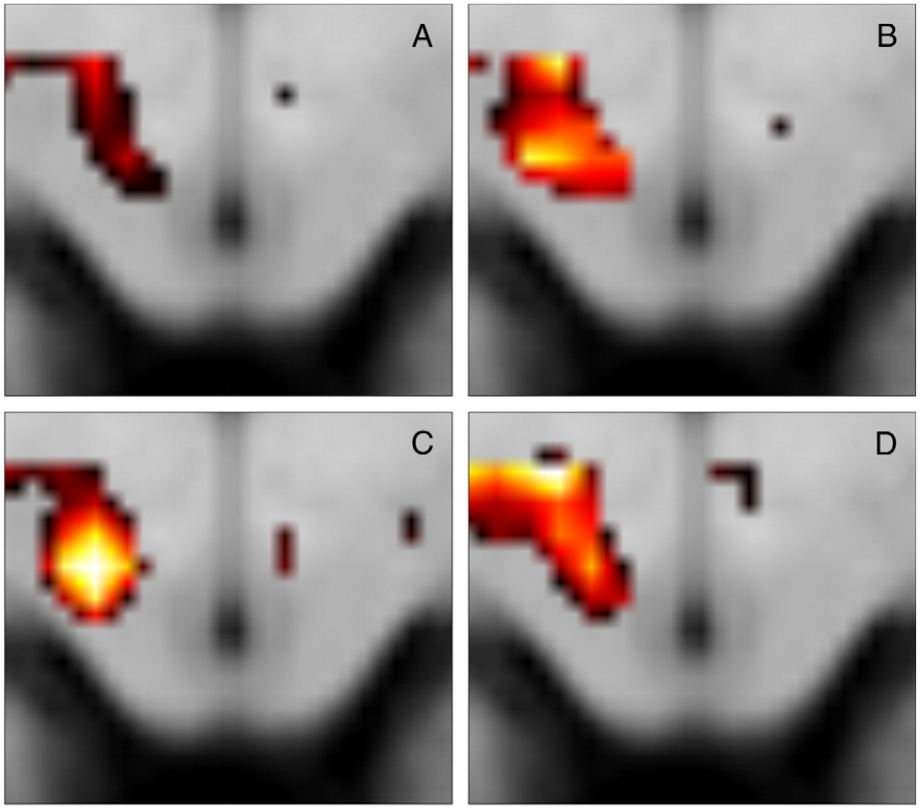

Fig. 2. Reach-related signal increases thresholded at $p = 0.001$ (uncorrected) and projected onto the group mean brain image at $z = -7$ mm (MNI coordinates). A, targets in the left visual field, pro-reaching; B, targets in the right visual field, anti-reaching; C, targets in the right visual field, pro-reaching; D, targets in the left visual field, anti-reaching.

Table 1
Individual MNI coordinates of the four SC regions for all participants: superficial/intermediate (si) and deep (d) positions of the left SC (SCL) and of the right SC (SCR). Mean: mean coordinates across the group with standard deviation. L&H 2012: group coordinates reported in Linzenbold and Himmelbach (2012). Please note that individual dSCL peaks were simply mirrored to the right side to provide dSCR peaks. This procedure was chosen because no signal changes could be detected at dSCR in whole volume contrasts.

Subject	siSCL			siSCR			dSCL		
	x	y	z	x	y	z	x	y	z
1	−6	−34	−4	4	−32	−4	−4	−28	−6
2	−2	−32	−4	4	−34	−4	−6	−28	−8
3	−4	−34	−4	6	−32	−4	−6	−28	−6
4	−4	−32	−2	4	−32	−4	−6	−28	−6
5	−4	−34	−4	4	−32	−4	−6	−28	−8
6	−4	−32	−4	4	−32	−4	−6	−28	−6
7	−2	−32	−4	4	−32	−4	−6	−28	−6
8	−6	−32	−2	4	−32	−6	−6	−28	−8
9	−4	−34	−4	4	−34	−4	−8	−28	−6
10	−4	−34	−2	4	−34	−4	−8	−28	−8
11	−2	−34	−4	4	−34	−4	−6	−28	−6
12	−4	−32	−4	4	−32	−4	−6	−28	−6
13	−4	−32	−4	4	−34	−4	−6	−28	−8
14	−4	−34	−2	4	−34	−4	−6	−28	−6
15	−4	−32	−4	2	−32	−4	−4	−28	−4
16	−4	−34	−4	2	−34	−4	−8	−28	−6
Mean (SD)	−3.9 (1.1)	−33 (1.0)	−3.5 (0.9)	3.9 (0.9)	−32.9 (1.0)	−4.1 (0.5)	−6.1 (1.1)	−28.0 (0)	−6.5 (1.2)
L&H 2012	−4	−32	−2	4	−32	−4	−6	−28	−6

0.12, $p = 0.73$) but 95% CIs substantiated the positive signal change for all conditions. The right dSC ROI showed a fundamentally different pattern, all time courses fluctuated around fixation baseline levels (Fig. 3D) and, again, the 2 × 2 ANOVA showed no significant differences between conditions (hemifield: $F_{1,15} = 0.42$, $p = 0.52$; congruency: $F_{1,15} = 0.11$, $p = 0.74$; interaction: $F_{1,15} = 2.18$, $p = 0.16$).

These results were most likely not influenced by systematic differences in the covariates of no interest. We analysed potential differences in the six motion regressors and the white matter regressors between conditions by calculating the average change of each regressor per condition and could not identify any significant differences between conditions (all $p \geq 0.08$; Table 2). Obviously, non-significant test outcome

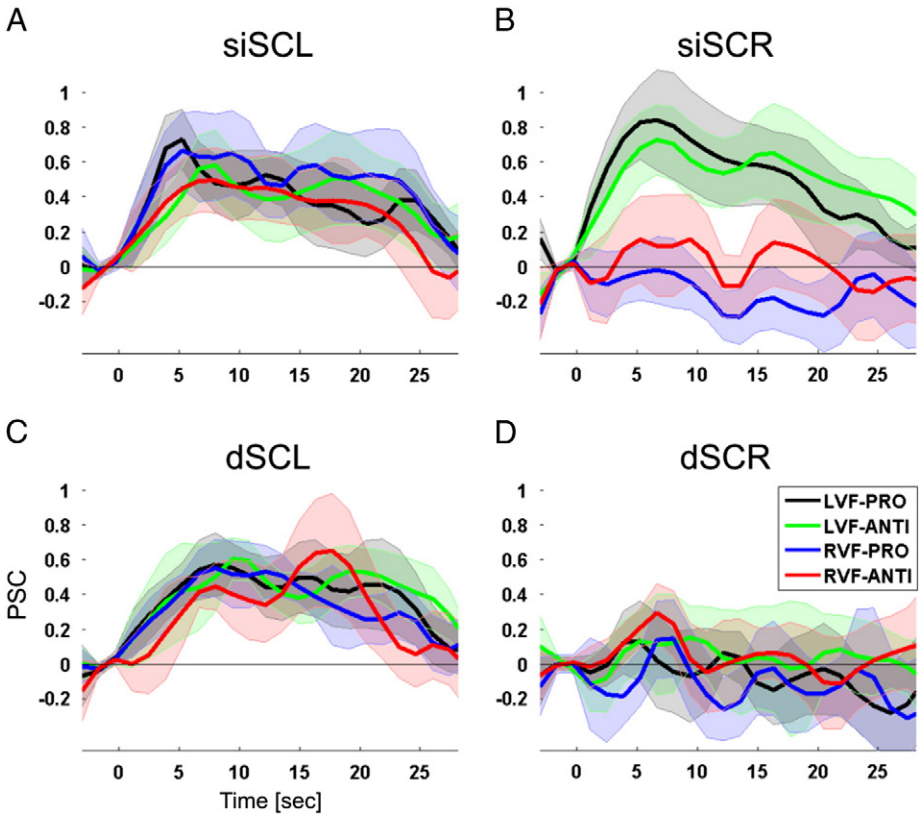

Fig. 3. Group signal time courses in the regions of interest. The average time course for each condition is shown together with the area of 95% confidence intervals. Time courses are synchronised to reaching block onset (0 s). A: time courses at the left superficial/intermediate superior colliculus (MNI group mean coordinates: −4 −33 −3). B: time courses at the right superficial/intermediate superior colliculus (4 −33 −4). C: time courses at the left deep superior colliculus (−6 −28 −7). D: time courses at the right deep superior colliculus (6 −28 −7).

Table 2
Condition-specific values of motion parameters and global white matter intensities. We calculated the differences between subsequent values corresponding to condition blocks and averaged the absolute values for each participant. Together with these mean values we report the 95% confidence limits and the results of a 2 (left vs. right targets) × 2 (pro- vs. anti-reach) repeated-measures ANOVA.

	Translations											
	X (mm)				Y (mm)				Z (mm)			
Condition	LVF PRO	LVF ANTI	RVF PRO	RVF ANTI	LVF PRO	LVF ANTI	RVF PRO	RVF ANTI	LVF PRO	LVF ANTI	RVF PRO	RVF ANTI
Mean	0.053	0.051	0.052	0.052	0.044	0.045	0.046	0.043	0.039	0.04	0.038	0.038
95% CI upper	0.044	0.043	0.044	0.044	0.036	0.034	0.035	0.035	0.033	0.031	0.031	0.032
95% CI lower	0.061	0.058	0.060	0.060	0.052	0.056	0.056	0.051	0.045	0.047	0.046	0.044
Visual field	$F(1,15) = 0.10$; $p < 0.76$				$F(1,15) = 0.001$; $p < 0.99$				$F(1,15) = 3.15$; $p < 0.10$			
Congruency	$F(1,15) = 1.34$; $p < 0.26$				$F(1,15) = 0.46$; $p < 0.51$				$F(1,15) = 0.07$; $p < 0.80$			
Interaction	$F(1,15) = 0.65$; $p < 0.43$				$F(1,15) = 3.4$; $p < 0.09$				$F(1,15) = 0.17$; $p < 0.69$			
	Rotations											
	Pitch (°)				Roll (°)				Yaw (°)			
Condition	LVF PRO	LVF ANTI	RVF PRO	RVF ANTI	LVF PRO	LVF ANTI	RVF PRO	RVF ANTI	LVF PRO	LVF ANTI	RVF PRO	RVF ANTI
Mean	0.0006	0.0006	0.0006	0.0005	0.0005	0.0005	0.0005	0.0005	0.0004	0.0004	0.0004	0.0004
95% CI upper	0.0004	0.0004	0.0004	0.0004	0.0004	0.0004	0.0004	0.0004	0.0004	0.0004	0.0004	0.0004
95% CI lower	0.0007	0.0007	0.0007	0.0006	0.0005	0.0005	0.0005	0.0005	0.0005	0.0005	0.0005	0.0005
Visual field	$F(1,15) = 0.001$; $p < 0.99$				$F(1,15) = 0.001$; $p < 0.99$				$F(1,15) = 2.68$; $p < 0.12$			
Congruency	$F(1,15) = 0.40$; $p < 0.54$				$F(1,15) = 1.39$; $p < 0.26$				$F(1,15) = 0.09$; $p < 0.77$			
Interaction	$F(1,15) = 2.28$; $p < 0.15$				$F(1,15) = 0.98$; $p < 0.34$				$F(1,15) = 0.09$; $p < 0.77$			

	White matter signal			
Condition	LVF PRO	LVF ANTI	RVF PRO	RVF ANTI
Mean	0.67	0.62	0.63	0.63
95% CI upper	0.59	0.58	0.56	0.57
95% CI lower	0.74	0.69	0.69	0.70
Visual field	$F(1,15) = 1.95$; $p < 0.18$			
Congruency	$F(1,15) = 3.52$; $p < 0.08$			
Interaction	$F(1,15) = 1.71$; $p < 0.21$			

cannot prove equivalence of the respective values. Therefore, we also present confidence intervals in Table 2 to give some impression of the size of possible differences.

Discussion

In good agreement with our previous results we found reach related BOLD signal increases in the dorsal and ventral locations of the SC contralateral to the active arm. Beyond our previous work we showed that also signal changes in the contralateral dorsal locations were driven by the execution of arm movements irrespective of retinotopic target positions. In contrast, visual stimulation alone predicted signal increases only in the dorsal SC hemisphere contralateral to the stimulated hemifield.

The results of the current study further supported the lateralisation of reach-related signals observed in Linzenbold and Himmelbach (2012). In our previous two experiments we examined two independent groups, the participants in one group moved the right arm, participants in the other group moved the left arm. Whereas reaching with the right arm correlated with signal increases in the left deep SC, reaching with the left arm correlated with increases in the right deep SC. The detailed inspection of signal timecourses already suggested that the ipsilateral deep SC was almost silent in terms of a BOLD response (Fig. 5 in Linzenbold and Himmelbach, 2012). However, the selection of the respective regions of interest were biased by the voxel-wise group analysis. The independent region of interest data presented here represent an exact replication of the results in experiment 1 reported in Linzenbold and Himmelbach (2012). The current data even lend additional support for a clear lateralisation of reach-related signals by a null-finding for the ipsilateral deep SC that is based on an unbiased ROI selection and calculations of confidence intervals. Unfortunately, a direct comparison to neurophysiological data from macaques is not possible as the lateralisation of reach-related signals was never directly examined in non-human primates. Measurements were usually restricted to the SC contralateral to the active limb. However, this was presumably done to maximise the number of successful recordings. Thus, this methodological decision by itself lends further support to a limb-related lateralisation pattern in the SC. Recently, Borra et al. (in press) examined connections between the premotor cortex and the region of the anterior intraparietal sulcus to the SC. Both cortical areas of the hand motor network showed a clear lateralisation with respect to the active hand in BOLD fMRI (Blangero et al., 2009). Borra et al. (in press) reported rich and extensive ipsilateral anterograde labelling after injections into the right or left cortical areas, whereas contralateral labelling was present but "considerably less rich and extensive". Thus, also the pattern of corticotectal connections suggests a limb-related lateralisation pattern of reach-related neurons in the SC.

Our results on the effects of visual stimulation alone are consistent with the reported topography of visual maps in the non-human SC (Cynader and Berman, 1972). This topography was also already demonstrated in humans several times (DuBois and Cohen, 2000; Linzenbold et al., 2011; Oldfield et al., 2012; Schneider and Kastner, 2005) and our data provide another confirmation of this pattern using fMRI. The presence of reach-related signals in the dorsal SC contralateral to the moving arm is consistent with our previously reported data (Linzenbold and Himmelbach, 2012). It is also consistent with the anatomical distribution of gaze independent reach-related neurons throughout the whole SC (Stuphorn et al., 2000) taking into account the spatial resolution of our fMRI data. Since the first reports, several different types of reach-related neurons in the SC

have been reported. Stuphorn et al. (2000) reported neurons that discharged only when monkeys reached for targets in a specific position relative to the gaze axis irrespective of the active arm. More recently, other studies provided evidence for SC neurons that are involved in the so-called "gaze anchoring" during eye–hand coordination in reaching (Reyes-Puerta et al., 2010, 2011). Obviously, we cannot differentiate between these different populations in the present experiment.

Considering previous reports on anti-saccades and anti-reaching, one might wonder why the results are so similar for both conditions. Behavioural studies of anti-reaching and anti-saccades consistently reported increased response latencies (reaching: Carey et al. (1996), Heath et al. (2009); saccades: Fischer and Weber (1992), Klein and Foerster (2001)). For anti-saccades, these increased latencies are considered to reflect the initial inhibition of a reflexive pro-saccade and the subsequent spatial transformations required to provide anti-saccade coordinates. Electrophysiological data in non-human primates supported this interpretation (Everling et al., 1999); for a review please see Munoz and Everling (2004). We found similar behavioural differences between pro- and anti-reaching. Therefore, we might also expect similar differences in the BOLD signals in the human SC. However, the extremely small temporal differences between pro- and anti-reaching make it unlikely that the analysis of human BOLD data, with a temporal resolution of several hundreds of milliseconds at best, could ever resolve such a serial process.

To conclude, we confirmed the involvement of the ventral human SC in the execution of arm movements. Beyond our previous results we demonstrated that active arm movements predicted signals in the dorsal SC contralateral to the moving arm in the absence of contralateral visual stimulation or eye movements. These results are in good agreement with the anatomical distribution of reach-related neurons in the SC of macaques.

Acknowledgments

This work was supported by the European Union (ERC StG 211078) and the Deutsche Forschungsgemeinschaft (HI 1371/1-1). We are grateful to Michael Erb and Uwe Klose from the Department of Neuroradiology for their technical support.

Conflict of interest statement

The authors have no conflict of interest to disclose.

References

Blangero, A., Menz, M.M., McNamara, A., Binkofski, F., 2009. Parietal modules for reaching. Neuropsychologia 47, 1500–1507.

Borra, E., Gerbella, M., Rozzi, S., Tonelli, S., Luppino, G., 2013. Projections to the superior colliculus from inferior parietal, ventral premotor, and ventrolateral prefrontal areas involved in controlling goal-directed hand actions in the macaque. Cereb. Cortex (in press).

Brett, M., Anton, J.-L., Valabregue, R., Poline, J.-B., 2002. Region of interest analysis using an SPM toolbox. Neuroimage 16.

Carey, D.P., Hargreaves, E.L., Goodale, M., 1996. Reaching to ipsilateral or contralateral targets: within-hemisphere visuomotor processing cannot explain hemispatial differences in motor control. Exp. Brain Res. 112, 496–504.

Cynader, M., Berman, N., 1972. Receptive-field organization of monkey superior colliculus. J. Neurophysiol. 35, 187–201.

DuBois, R.M., Cohen, M.S., 2000. Spatiotopic organization in human superior colliculus observed with fMRI. Neuroimage 12, 63–70.

Everling, S., Dorris, M.C., Klein, R.M., Munoz, D.P., 1999. Role of primate superior colliculus in preparation and execution of anti-saccades and pro-saccades. J. Neurosci. 19, 2740–2754.

Fischer, B., Weber, H., 1992. Characteristics of "anti" saccades in man. Exp. Brain Res. 89, 415–424.

Heath, M., Maraj, A., Gradkowski, A., Binsted, G., 2009. Anti-pointing is mediated by a perceptual bias of target location in left and right visual space. Exp. Brain Res. 192, 275–286.

Jay, M.F., Sparks, D.L., 1987. Sensorimotor integration in the primate superior colliculus. II. Coordinates of auditory signals. J. Neurophysiol. 57, 35–55.

Klein, C., Foerster, F., 2001. Development of prosaccade and antisaccade task performance in participants aged 6 to 26 years. Psychophysiology 38, 179–189.

Linzenbold, W., Himmelbach, M., 2012. Signals from the deep: reach-related activity in the human superior colliculus. J. Neurosci. 32, 13881–13888.

Linzenbold, W., Lindig, T., Himmelbach, M., 2011. Functional neuroimaging of the oculomotor brainstem network in humans. Neuroimage 57, 1116–1123.

Lünenburger, L., Kleiser, R., Stuphorn, V., Miller, L.E., Hoffmann, K.P., 2001. A possible role of the superior colliculus in eye–hand coordination. Prog. Brain Res. 134, 109–125.

Munoz, D.P., Everling, S., 2004. Look away: the anti-saccade task and the voluntary control of eye movement. Nat. Rev. Neurosci. 5, 218–228.

Oldfield, E.H., et al., 2012. Identification and characterisation of midbrain nuclei using optimised functional magnetic resonance imaging. Neuroimage 59, 1230–1238.

Reyes-Puerta, V., Philipp, R., Lindner, W., Hoffmann, K.P., 2010. Role of the rostral superior colliculus in gaze anchoring during reach movements. J. Neurophysiol. 103, 3153–3166.

Reyes-Puerta, V., Philipp, R., Lindner, W., Hoffmann, K.P., 2011. Neuronal activity in the superior colliculus related to saccade initiation during coordinated gaze-reach movements. Eur. J. Neurosci. 34, 1966–1982.

Schneider, K.A., Kastner, S., 2005. Visual responses of the human superior colliculus: a high-resolution functional magnetic resonance imaging study. J. Neurophysiol. 94, 2491–2503.

Stein, B.E., Wallace, M.W., Stanford, T.R., Jiang, W., 2002. Cortex governs multisensory integration in the midbrain. Neuroscientist 8, 306–314.

Stuphorn, V., Bauswein, E., Hoffmann, K.P., 2000. Neurons in the primate superior colliculus coding for arm movements in gaze-related coordinates. J. Neurophysiol. 83, 1283–1299.

Wall, M.B., Walker, R., Smith, A.T., 2009. Functional imaging of the human superior colliculus: an optimised approach. Neuroimage 47, 1620–1627.

Werner, W., Dannenberg, S., Hoffmann, K.P., 1997a. Arm-movement-related neurons in the primate superior colliculus and underlying reticular formation: comparison of neuronal activity with EMGs of muscles of the shoulder, arm and trunk during reaching. Exp. Brain Res. 115, 191–205.

Werner, W., Hoffmann, K.P., Dannenberg, S., 1997b. Anatomical distribution of arm-movement-related neurons in the primate superior colliculus and underlying reticular formation in comparison with visual and saccadic cells. Exp. Brain Res. 115, 206–216.